

3D meso-scale modeling of concrete with a local background grid method

Hao Ouyang ^a, Xiaowei Chen ^{b,c,*}

^a Institute of Computer Application, China Academy of Engineering Physics, Mianyang 621999, Sichuan, China

^b Advanced Research Institute of Multidisciplinary Science, Beijing Institute of Technology, Beijing 100081, China

^c State Key Lab of Explosion Science and Technology, Beijing Institute of Technology, Beijing 100081, China



HIGHLIGHTS

- A novel method is proposed to generate the 3D meso-scale model of concrete.
- The meso-modeling process is simplified and the calculation efficiency is improved.
- A large amount of aggregate intrusion detection is avoided in local background grids.
- The aggregate content is higher and the shape of the aggregate is unlimited.
- Uniaxial compression and projectile penetration of meso-concrete are well simulated.

ARTICLE INFO

Article history:

Received 31 July 2019

Received in revised form 4 February 2020

Accepted 27 April 2020

Available online 19 May 2020

Keywords:

Concrete

Meso-modelling

Local background grid

Random aggregate

ABSTRACT

Concrete is a three-phase heterogeneous composite material composed of aggregate, cement mortar and its bonding interface. The complex meso-structure of concrete has a direct influence on its macroscopic mechanical properties. In this paper, a new efficient method of concrete meso-modelling is proposed based on the local background grid method. The random polyhedral aggregate is generated according to aggregate gradation and dropped directly into the background mesh one by one. The process of concrete meso-modelling is simplified compared with the traditional meso-scale model of concrete. According to the aggregate shape and its spatial position, the newly placed aggregate is encapsulated by a bounding box, in which the identification of concrete meso-components and intrusion detection of new and old aggregates are carried out. By transforming aggregate intrusion detection during the process of concrete meso-geometric modeling into overlap check of aggregate elements in the local background grid, a large number of disjoint conditions between new and old aggregates are avoided. Thus a large amount of global calculation is greatly reduced, and the efficiency of concrete meso-modelling is obviously improved. The effects of aggregate element content, element mesh size and aggregate particle size distribution on concrete meso-modelling are analyzed. Finally, the reliability and validity of the concrete meso-model are verified by numerical simulation of concrete uniaxial compression and projectile penetration into concrete.

© 2020 Elsevier Ltd. All rights reserved.

1. Introduction

Concrete is the most widely used building material in the world, and has a large number of applications in the field of structural engineering. As a complex heterogeneous composite material, concrete can be regarded as a three-phase composite structure composed of aggregate, cement mortar and its interface transition zone (ITZ) at the mesoscopic level. The mechanical properties

and failure modes of concrete are closely related to its mesoscale material components and mesoscale structure [1]. Therefore, a mesoscopic model with explicit representation of the actual meso-structure of concrete is needed to analyze the relationship between mesoscale structure and macroscopic mechanical behavior of concrete, which is a hot issue in the numerical simulation research of concrete at present.

Generally speaking, the concrete meso-model is divided into two steps: first, the meso-scale geometric model of concrete is established, and then the meso-scale geometric model is meshed to obtain the meso-scale finite element model. Based on the existing literature in recent years, the methods of generating meso-scale

* Corresponding author at: Advanced Research Institute of Multidisciplinary Science, Beijing Institute of Technology, Beijing 100081, China.

E-mail address: chenxiaoweintu@bit.edu.cn (X. Chen).

geometric model of concrete can be summarized as three kinds: random aggregate placement method [2–6], Voronoi graphic method [7–10,11], and CT scanning method [12,13].

The random aggregate placement method is to randomly place the pre-generated random aggregate into the target geometric region of the specimen, thus obtaining a meso-scale geometric model of concrete. The advantage of this method is that it can meet the requirements of aggregate shape, aggregate size and aggregate gradation distribution. However, for this method, due to the randomness of the placing process and the large amount of intrusion detection of aggregates, the normal process of “take-and-place” is very time-consuming and it is difficult to achieve a higher aggregate content [4]. Some literatures use various methods to raise the volume fraction of aggregates, such as “occupation and removal method” [4] to improve placement efficiency and “creation of supplementary aggregates” [11] to directly increase the aggregate content.

The Voronoi graphic method is based on the three-dimensional Voronoi technique, which divides the geometric region of concrete specimens into several adjacent polyhedrons, and then separates these polyhedrons by “shrinking” to obtain solitary polyhedrons to characterize concrete aggregates. Generally speaking, the two-phase meso-scale geometric model of concrete, containing only aggregate and mortar generated by the Voronoi graphics method, can have an aggregate content of up to 80% [7,11]. If ITZ is further considered, the aggregate content will be reduced to about 70%. This method can obtain high aggregate content and good aggregate shape, but it is difficult to satisfy the predetermined aggregate gradation distribution.

The CT scanning method performs the three-dimensional reconstruction based on the CT scanning images of concrete sections, which can reflect the actual meso-structure of the concrete, but the whole process is time-consuming and expensive. In addition, the aggregate shape, aggregate content, and the distinction of the ITZ layer are all closely related to the resolution of the CT scan.

The methods of discretizing the meso-scale geometric model of concrete to generate its meso-scale finite element model mainly include the direct meshing method [14,15] and the background grid mapping method [2–4]. Direct meshing of the meso-scale geometric model of concrete can better preserve the shape of the concrete aggregate. However, due to the randomness of aggregate size and shape, the mesh quality is difficult to control, which ultimately affects the accuracy of the solution. The background mesh mapping method generates uniform background grids in the space occupied by concrete geometric model, then identifies the material attribute of each background mesh element, and finally obtains meso-scale finite element model of concrete. The advantage of this method is that it can obtain uniform hexahedral computational grids and improve the computational efficiency. However, the accuracy of aggregate surface profile depends on the fineness of the background grid.

This paper proposed a new method to directly and efficiently generate the meso-scale finite element model of concrete. The present method combines the random aggregate placement method and the background grid mapping method. The generated aggregate is directly put into the background mesh, and the meso-scale geometric modeling of concrete and the meso-scale finite element modeling of concrete are simplified as one step. In addition, the local background grid method is used to locate and encapsulate the randomly placed aggregate, and then the selection of concrete meso-components and aggregate collision check are completed in the local background grid. This avoids a lot of disjoint judgement calculations of polyhedrons and improves the efficiency of concrete meso-modeling.

2. Aggregate gradation and the global background grid initialization

2.1. Aggregate gradation

Concrete aggregate can be divided into coarse aggregate and fine aggregate according to its particle size. The particle size of coarse aggregate is usually larger than 5 mm, and its volume fraction accounts for 40% ~ 50% of the total volume of concrete [16]. The aggregate content of concrete is closely related to the size distribution of aggregates, which directly affects the macroscopic mechanical properties of concrete. The particle size distribution of the aggregate can be determined according to the ideal gradation curve of the maximum density of concrete aggregate proposed by Fuller et al. [17].

$$P(d) = 100 \left(\frac{d}{d_{\max}} \right)^n \quad (1)$$

where $P(d)$ represents the cumulative volume fraction of aggregates with a particle size less than d , and d_{\max} denotes the maximum aggregate particle size. The aggregate gradation curve of concrete is shown in Fig. 1. The empirical exponent n is usually between 0.45 and 0.70. In this paper, n is taken as 0.5. However, the program in this paper also supports user-defined aggregate gradation distribution.

According to Eq. (1), the volume fraction of aggregates with particle size between $[d_i, d_{i+1}]$ is:

$$\nu_{[d_i, d_{i+1}]} = \frac{P(d_{i+1}) - P(d_i)}{P(d_{\max}) - P(d_{\min})} \times \nu_p \quad (2)$$

where d_{\max} and d_{\min} represent the maximum and minimum aggregate particle sizes in the current gradation, respectively, and ν_p represents the total aggregate content. The common gradation distribution of concrete aggregate is shown in Table 1.

2.2. Initialization of the global background grid

The global background grid of concrete specimen with a three-dimensional size $L \times W \times H$ is initialized to generate uniform structural grids. Firstly, the mesh element size e should be determined. If the size of mesh element is too small, it will greatly increase the amount of unnecessary storage and calculation. However, if the mesh element size is too large, the meso-geometric shape and boundary of aggregates cannot be fully depicted. According to the actual three-dimensional meso-modelling of con-

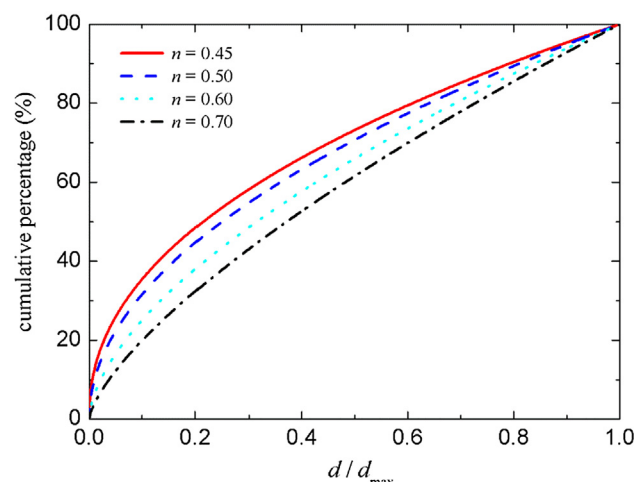


Fig. 1. The aggregate gradation curve of concrete.

Table 1

Common concrete aggregate gradation distribution.

aggregate size/mm	aggregate type	aggregate gradation	aggregate proportion
5 ~ 20	small	1st gradation	1 : 0 : 0 : 0
20 ~ 40	medium	2nd gradation	5.5 : 4.5 : 0 : 0
40 ~ 80	large	3rd gradation	3 : 3 : 4 : 0
80 ~ 150	huge	4th gradation	2 : 2 : 3 : 3

crete, the mesh element size e is generally taken as $1/4 \sim 1/8$ of the minimum aggregate particle size d_{\min} .

According to the mesh element size, the total number of elements in the three-dimensional direction of the global background grid can be determined as $l \times m \times n$, where $l = L/e$, $m = W/e$, $n = H/e$, and $/\backslash$ denotes exact division. Therefore, the actual size in the three-dimensional direction of the global background grid is $le \times me \times ne$. The initialization of the global background grid of concrete specimen is shown in Fig. 2. For any element (i, j, k) in the global background grid, the coordinates of its eight nodes can be determined as follows:

$$\begin{aligned} & (ie, je, ke); ((i+1)e, je, ke); (ie, (j+1)e, ke); ((i+1)e, (j+1)e, ke) \\ & (ie, je, (k+1)e); ((i+1)e, je, (k+1)e); (ie, (j+1)e, (k+1)e); \\ & ((i+1)e, (j+1)e, (k+1)e) \end{aligned} \quad (3)$$

The coordinates of the central point of any element (i, j, k) are:
 $(ie + e/2, je + e/2, ke + e/2)$ (4)

Accordingly, if the coordinates of any point in the background mesh block are (x, y, z) , the number of the element where the point is located can also be obtained as follows:

$$(x/e, y/e, z/e) \quad (5)$$

A three-dimensional matrix M_{ijk} ($0 \leq i \leq l-1$, $0 \leq j \leq m-1$, $0 \leq k \leq n-1$) is used to store the material attributes of all the global background elements. In this paper, $M_{ijk} = 1, 2, 3$ means that the grid element (i, j, k) is a mortar element, an ITZ element or an aggregate element, respectively.

Before the beginning of aggregate placement, the material attributes of all the global background elements are initialized to be as mortar. As the aggregate is successfully placed into the global background grid one by one, the material attributes of the corresponding elements will be constantly changed until the aggregate content reaches the expected value. Finally, according to the element information in the global background grid, the meso-scale finite element model of concrete is directly generated.

3. Random placement of aggregates based on the local background grid

3.1. Generation of random polyhedral aggregate

The aggregate in actual concrete is mostly pebble or gravel. Therefore, sphere, ellipsoid or random polyhedron are commonly used to simulate the geometry of aggregate in concrete. The generation of regular spherical or ellipsoidal aggregate is relatively simple, so the generation method of random polyhedral aggregates is mainly considered here. Random aggregates should reflect the randomness of the geometry of aggregate as far as possible and avoid excessive sharp angles and narrow patches. In this paper, random polyhedral aggregates are constructed based on spatial octahedral random growth algorithm [2,18,19]. The random growth algorithm is mainly divided into two steps: first, an octahedron aggregate base is generated in an auxiliary sphere, and then the octahedron aggregate base is extended based on its longest edge.

In order to obtain a higher aggregate content, aggregates are created and placed one by one according to the grading order of aggregates from large size to small size. Assuming that the aggregate size of the current gradation is d , the polyhedral aggregate will be generated in an auxiliary sphere. The center of the auxiliary sphere is located at the coordinate origin O and the radius r is $d/2$. Firstly, six vertices A_i ($i = 1, 2, \dots, 6$) of the random octahedron are established on the auxiliary sphere. The Cartesian coordinates of six vertices can be obtained from the azimuth angle φ and the inclination angle θ of the spherical coordinates, as in Eq. (6).

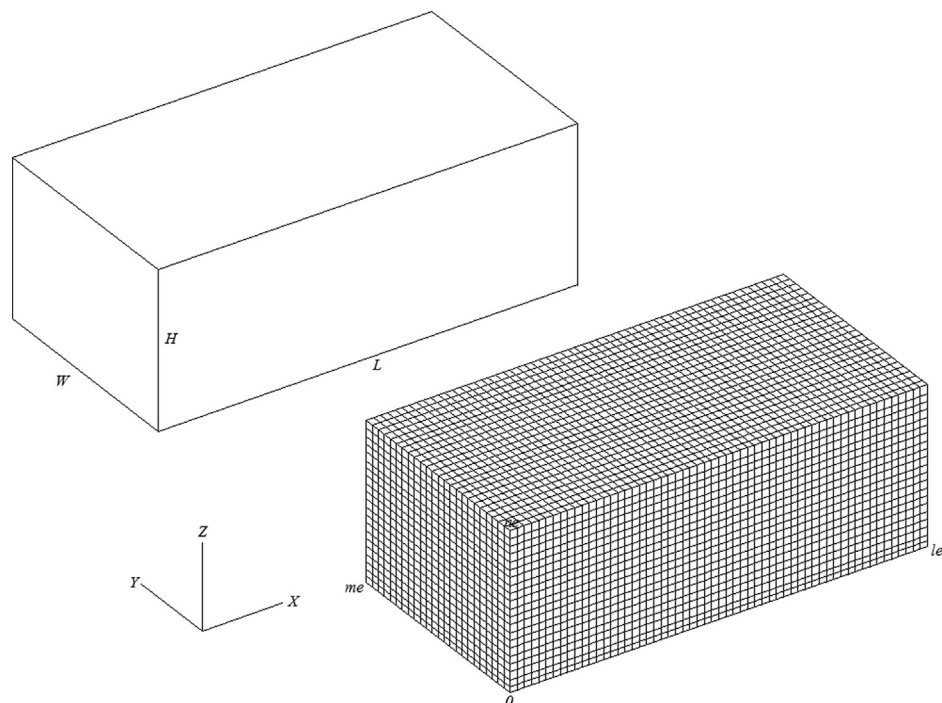


Fig. 2. The global background grid of concrete specimen.

$$x_i = r \sin \theta_i \cos \varphi_i, \quad y_i = r \sin \theta_i \sin \varphi_i, \quad z_i = r \cos \theta_i \quad (6)$$

In order to control the shape of the octahedral aggregate and avoid sharp angles, it is necessary to limit the azimuth angle φ and the inclination angle θ of six vertices. The first four vertices are on the horizontal circle of the auxiliary sphere, and the latter two vertices are on the upper and lower hemispheres respectively, as in Eq. (7), where η_i , χ_i and χ_6 are random numbers between [0, 1].

$$\begin{aligned} \varphi_i &= (i-1)\pi/2 + \eta_i\pi/2 & (i=1,2,3,4) \\ \varphi_{i+1} - \varphi_i &\geq \pi/4, & 2\pi + \varphi_1 - \varphi_4 \geq \pi/4 \quad (i=1,2,3) \\ \theta_i &= \pi/2 & (i=1,2,3,4) \\ \varphi_i &= 2\pi\eta_i & (i=5,6) \\ \theta_5 &= \chi_5\pi/4, \theta_6 = 3\pi/4 + \chi_6\pi/4 & \end{aligned} \quad (7)$$

Secondly, the octahedron grows randomly as follows: find the longest side A_iA_j of the octahedron and M is its midpoint; create a new vertex A_7 randomly on the extension line of OM , and the new point A_7 satisfies: $0.1|A_iA_j| < |MA_7| < 0.5|A_iA_j|$. A new random decahedron is obtained by connecting the new vertex A_7 with the four vertices of the two planes on which the longest side A_iA_j is located. Similarly, any random polyhedral aggregate meeting the requirements can be obtained by further aggregate growth. In order to further improve the randomness of aggregates, the newly generated polyhedron can be randomly rotated around coordinate axes x , y and z at angles α , β and γ , respectively. Fig. 3 (a) is a random decahedron after one growth stage.

In addition, according to the Delaunay triangulation and the corresponding convex hull algorithm, a convex polyhedral aggregate can also be constructed based on a three-dimensional random point set [13], and the vertex coordinates and corresponding topological relations of the polyhedron can be obtained, as shown in Fig. 3(b). Eq. (8) is used to calculate the spherical coordinates of the three-dimensional random point set, and then the Cartesian coordinates of these points are calculated according to Eq. (6).

$$\begin{aligned} r_i &= d_k/2 + (d_{k+1}/2 - d_k/2)\eta_i \\ \theta_i &= 2\pi\eta_i \\ z_i &= 2\pi\eta_i \end{aligned} \quad (8)$$

where η_i is a random number between [0, 1] and $[d_k, d_{k+1}]$ is the aggregate size range of the current gradation. The number of three-dimensional random points is preferably controlled between 15 and 25.

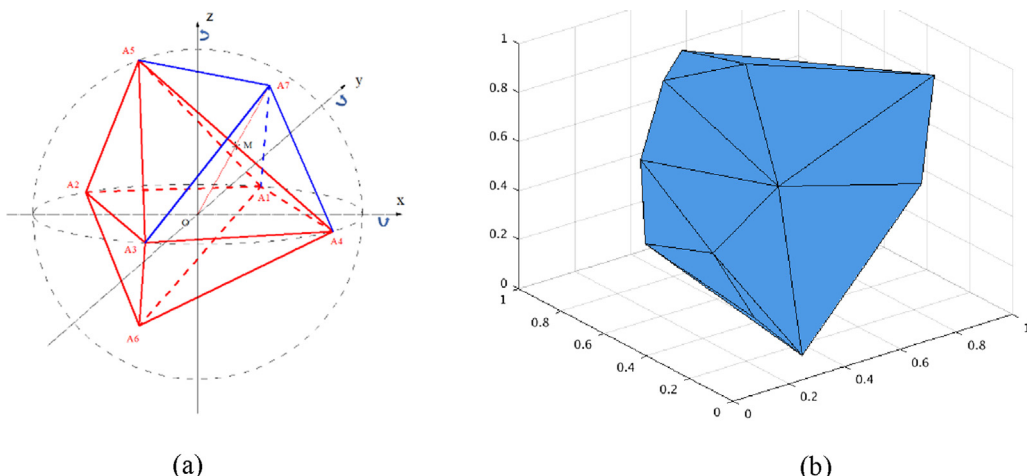


Fig. 3. Methods for creating the polyhedral aggregate. (a) random growth of octahedral. (b) convex hull of 20 random points.

3.2. Aggregate random placement and the local background grid

The local background grid is a dynamic bounding box related to the location and shape of the current aggregate, in which element attribute recognition and aggregate intrusion detection are performed.

(1) Determination of the random placement location of aggregate

The newly generated random polyhedral aggregate is directly put into the background grid space by a random translation. Assuming that the coordinates of the N vertices of the polyhedral aggregate are (x_i, y_i, z_i) , $0 \leq i \leq N-1$, and the coordinates of the random translation point P are $(x_p, y_p, z_p) = (\eta_7 le, \eta_8 me, \eta_9 ne)$, where η_7, η_8 and η_9 are random numbers between [0, 1]. Therefore, the coordinates of all vertices of the aggregate after random translation are:

$$X_i = x_i + x_p, \quad Y_i = y_i + y_p, \quad Z_i = z_i + z_p \quad (0 \leq i \leq N-1) \quad (9)$$

According to the different preparation methods of concrete specimens, the boundary conditions for aggregate random placement are also different. For a concrete block cut from an entire concrete specimen, it only needs to ensure that the random translation point P is in the space of the concrete specimen. For an entire concrete specimen, it needs to control all the vertices (X_i, Y_i, Z_i) of the randomly translated aggregate are in the space of the concrete specimen, namely

$$0 \leq X_i \leq le, \quad 0 \leq Y_i \leq me, \quad 0 \leq Z_i \leq ne \quad (0 \leq i \leq N-1) \quad (10)$$

To further improve the efficiency of aggregate random placement, the random translation point P can be controlled to fall inside the mortar elements. That is to say, the material attribute value of the element where the random translation point P is located should be 1.

(2) Determination of the local background grid

According to the new coordinates of the vertices of the polyhedral aggregate by Eq. (9), the minimum values ($X_{\min}, Y_{\min}, Z_{\min}$) and maximum values ($X_{\max}, Y_{\max}, Z_{\max}$) of all the vertex coordinates in the three-dimensional direction are obtained. The element numbers of the minimum and the maximum coordinates can be determined by Eq. (5).

$$\begin{aligned} (i_r, j_r, k_r) &= (X_{\min}/e, Y_{\min}/e, Z_{\min}/e) \\ (I_r, J_r, K_r) &= (X_{\max}/e, Y_{\max}/e, Z_{\max}/e) \end{aligned} \quad (11)$$

Considering a concrete block cut from an entire concrete specimen, some vertices of the polyhedral aggregate may be outside the space of concrete block. Therefore, the bounding box of the newly placed aggregate should be determined by Eq. (12).

$$(i_r, j_r, k_r) = (\max(0, X_{\min}/e), \max(0, Y_{\min}/e), \max(0, Z_{\min}/e))$$

$$(I_r, J_r, K_r) = (\min(l, X_{\max}/e), \min(m, Y_{\max}/e), \min(n, Z_{\max}/e))$$

$$(12)$$

In addition, because the interface transition zone (ITZ) between aggregate and mortar has an important influence on the mechanical properties of concrete, ITZ should be considered in the numerical modeling of concrete. However, the actual ITZ is very thin, with a thickness ranging from 10 to 50 μm . Due to the limitation of computational capacity, the mesh element size of the numerical model can hardly meet the size requirements of actual ITZ. In this paper, the method for generating ITZ is to take a layer of element cells of the outer contour of the aggregate as the ITZ elements. Consequently, the bounding box with considering the ITZ elements needs to be extended outward one more layer, namely

$$(i_b, j_b, k_b) = (\max(0, X_{\min}/e - 1), \max(0, Y_{\min}/e - 1), \max(0, Z_{\min}/e - 1))$$

$$(I_b, J_b, K_b) = (\min(l, X_{\max}/e + 1), \min(m, Y_{\max}/e + 1), \min(n, Z_{\max}/e + 1))$$

$$(13)$$

Taking the 2D case as an example, as shown in Fig. 4(a), the red dotted block indicates the bounding box of current aggregate, and the blue dotted block represents the bounding box further considering the ITZ elements. The grids within the bounding box are the corresponding local background grids.

3.3. Material attribute identification and aggregate intrusion detection

A three-dimensional dynamic matrix B is used to temporarily store the material attributes of the current local background grid. Matrix B is initialized to 1, that is, all elements in the local background grid are initialized as mortar elements. The corresponding relations between the elements in the local background grid matrix B and the elements in the global background grid matrix M are as follows:

$$\begin{array}{ccc} M & \text{global} & B & \text{local} \\ (i_b, j_b, k_b) & \iff & (0, 0, 0) \\ \vdots & & \vdots \\ (i + i_b, j + j_b, k + k_b) & \iff & (i, j, k) \\ \vdots & & \vdots \\ (I, J, K) & \iff & (I - i_b, J - j_b, K - k_b) \\ \vdots & & \vdots \\ (I_b, J_b, K_b) & \iff & (I_b - i_b, J_b - j_b, K_b - k_b) \end{array} \quad (14)$$

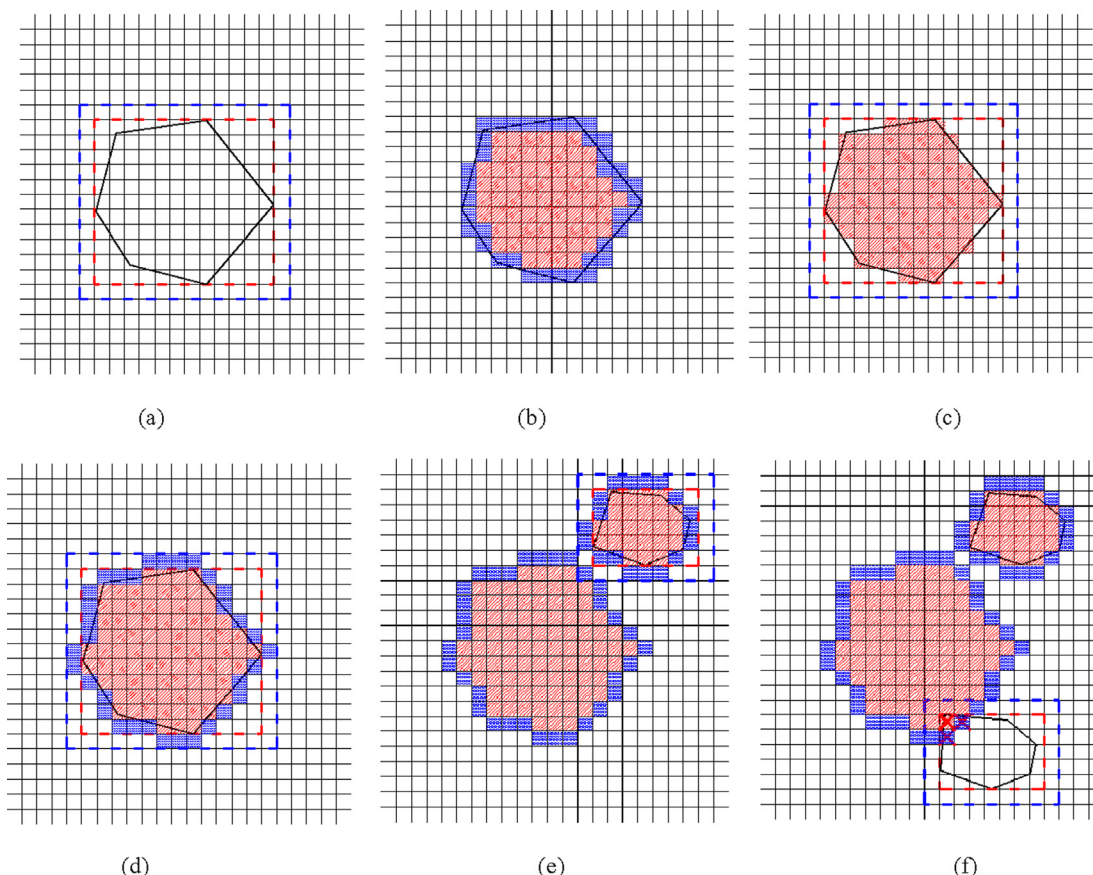


Fig. 4. Schematic view of meso-modeling of concrete based on the local background grid (2D case): (a) aggregate random placement and the corresponding local background grid. (b) the conventional identification method. (c) identification of aggregate elements (d) generation of ITZ elements. (e) add a new aggregate. (f) intrusion of new and old aggregate.

Any element (i, j, k) in the local background grid corresponds to the element $(i + i_b, j + j_b, k + k_b)$ in the global background grid, and any element (I, J, K) in the global background grid corresponds conversely to the element $(I - i_b, J - j_b, K - k_b)$ in the local background grid.

3.3.1. Material attribute identification

The material attributes are sequentially identified for all the elements in the local background grid according to the relative position relationship between the element and aggregate geometry. According to some literatures [2–4], the conventional method of identifying element material is:

- 1) All nodes of the element are inside the aggregate geometry, and then it is determined as an aggregate element.
- 2) All nodes of the element are outside the aggregate geometry, and then it is determined as a mortar element.
- 3) For other cases, the element is an ITZ element.

Fig. 4(b) is the result of meso-component identification of aggregate in **Fig. 4(a)** according to the above method. The red filling elements are aggregate elements and the blue filling elements are ITZ elements. Obviously, the total area of aggregate elements obtained by the conventional algorithm is much smaller than the actual aggregate geometry area, and the aggregate contour cannot be well depicted.

In order to better represent the outline of concrete aggregate, another identification method of concrete meso-components is proposed in this paper. The elements with the center point in the aggregate geometry are identified as aggregate elements, as shown in **Fig. 4(c)**. After the identification of aggregate elements, a layer of element cells of the outer outline of the meso-aggregate are selected as ITZ elements, as shown in **Fig. 4(d)**. Comparing **Fig. 4(c)** with **Fig. 4(d)**, it is clear that the mesoscopic aggregate model obtained by this method is in better agreement with the actual aggregate geometry.

The specific algorithm for identifying aggregate elements is as follows:

- 1) Loop through all the elements in the local background grid of current aggregate, i.e., all the elements in the red dotted block in **Fig. 4(a)**.
- 2) According to the element number of the local background grid, the corresponding element number of the global background grid is obtained, and then the coordinates of the element center point are obtained by Eq. (4). The relative position relationship between the center point and the aggregate geometry can be determined. If the center point is inside the aggregate geometry, this element in the local background grid will be determined as an aggregate element.

The specific algorithm for generating ITZ elements is as follows:

- 1) Loop through all the mortar elements in the local background grid, i.e., all the mortar elements in the blue dotted block in **Fig. 4(a)**.
- 2) The element will be determined to be an ITZ element if it is adjacent to an aggregate element.

3.3.2. Aggregate intrusion detection

The conventional aggregate intrusion detection occurs in the process of meso-scale geometric modeling of concrete. When a new random polyhedral aggregate is generated and placed into the space of concrete specimen, it has to check whether the new

aggregate intrude into any other aggregate. The conventional method of intrusion detection is complicated. With the increase of the number of aggregates, the amount of calculation becomes larger and larger, which greatly reduces the efficiency of concrete meso-modeling.

In this paper, the aggregate intrusion detection is quite simple, and it is integrated into the process of material attribute recognition of concrete meso-components. No overlap or contact between new and old aggregate is allowed. Therefore, we add a judgment during the process of identification of aggregate elements (as shown in **Section 3.3.1**): When a new element in the local background grid of the newly placed aggregate is judged as an aggregate element, this element cannot be an aggregate element or ITZ element of any other old aggregate. Otherwise, the intrusion occurs and we need to move the aggregate to a new random location and determine its new local background grid.

The detailed process is explained as follows: For any newly determined aggregate element (i, j, k) in the local background grid ($B_{ijk} = 3$), in order to ensure that the new aggregate element (i, j, k) does not overlap or contact with the old aggregate elements, its corresponding element $(i + i_b, j + j_b, k + k_b)$ in the global background grid cannot be an aggregate element or ITZ element, i.e., $M_{i+i_b, j+j_b, k+k_b} \neq 3$ or 2.

Fig. 4 shows the schematic views of aggregate random placement based on the local background grid in a 2D situation. If the above conditions are satisfied during the whole process of material attribute identification of new aggregate, then this new aggregate is placed successfully and the corresponding aggregate elements are identified, as shown in **Fig. 4(c)**. The ITZ elements are generated by selecting a single layer of elements around the aggregate particle, as shown in **Fig. 4(d)**. Finally, the aggregate and ITZ elements in the local background grid are updated to the global background grid. **Fig. 4(e)** shows the successful placement of a new aggregate. **Fig. 4(f)** shows the intrusion of new and old aggregates in a 2D situation.

4. Algorithm comparison and case analysis

4.1. Algorithm comparison

Fig. 5 and **Fig. 6** exhibit the concrete meso-modeling processes of the traditional method and the present method respectively. As can be seen from **Fig. 5** and **Fig. 6**, the present method directly establishes the meso-scale finite element model of concrete and simplifies the modeling process. The randomly generated polyhedral aggregate is directly put into the global background grid of the concrete space until the predefined aggregate content is reached, and the identification of concrete meso-components and aggregate intrusion check are both conducted in the local background grid. Two key steps in the conventional meso-modeling process including aggregate intrusion check and material attribute identification (red dotted boxes shown in **Fig. 5**) are integrated into one step of aggregate recognition and intrusion check based on the local background grid (blue dotted box shown in **Fig. 6**). Thus large amount of redundant calculation in the above two steps are reduced, which greatly improves the modeling efficiency. However, in the traditional method, time consumption is very huge in order to adjust the position of each aggregate one by one for avoiding intrusion between the new placing aggregate and all the old placed aggregates.

In order to evaluate the computational performance between the traditional method and the present method, simulations based on different methods are conducted to establish concrete meso-model with the same volume fraction of aggregates. The computational time of these different methods are shown in **Table 2**. It is

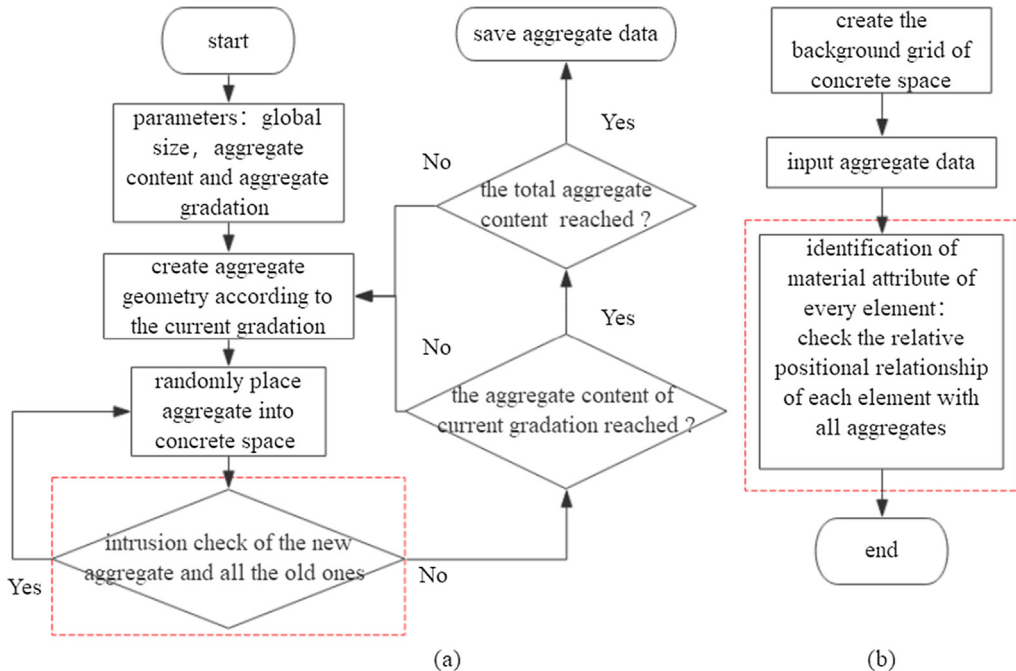


Fig. 5. Flowchart of the conventional concrete meso-modeling: (a) meso-scale geometric modeling, (b) meso-scale finite element modeling.

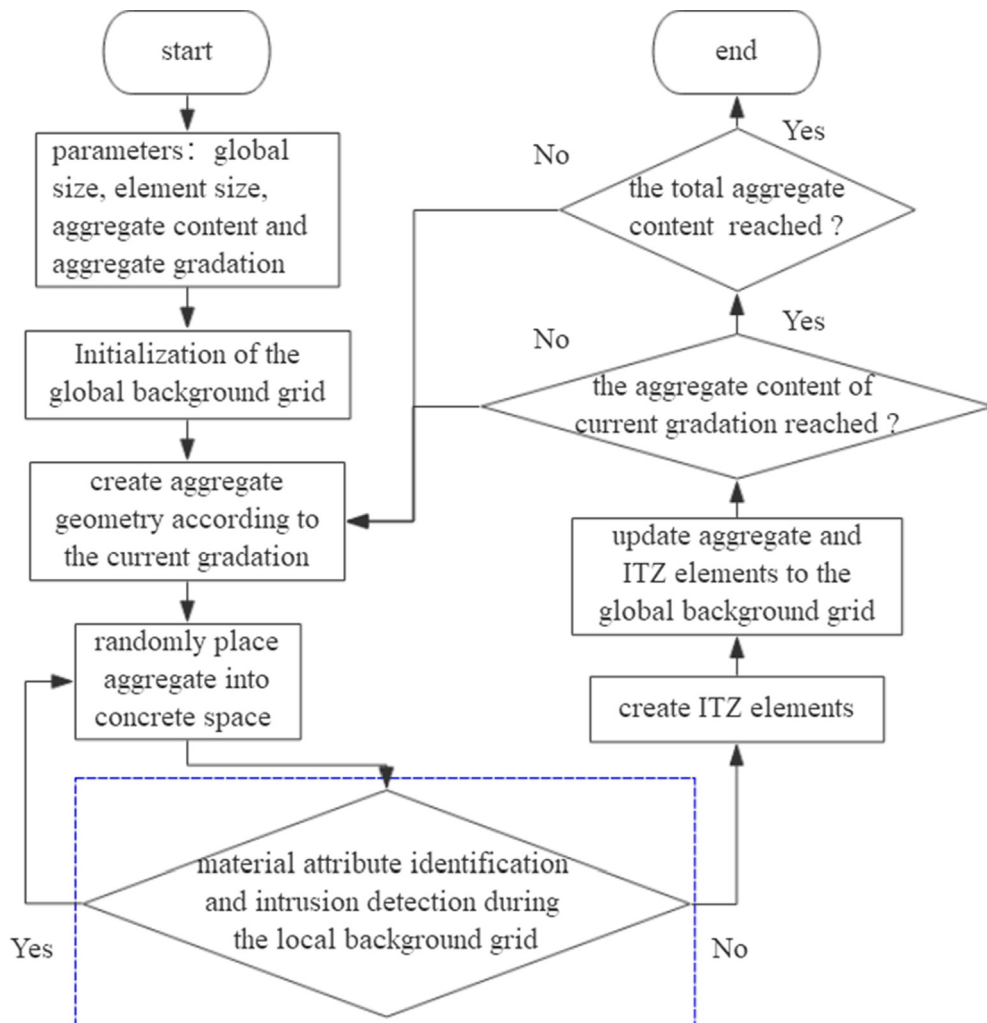


Fig. 6. Flowchart of concrete meso-modeling of the present method.

Table 2

The computational time (unit s) for generating concrete meso-model based on different methods.

Aggregate content	Voronoi-based method [11] time for generating geometric model	Traditional randomaggregate method [19]		Present method time for directly generating the finite element model
		time for generating geometric model	time for meshing the geometric model	
0.15	817	101	157	4
0.2	2518	135	221	5
0.25	/	216	290	8
0.3	/	407	344	12
0.35	/	1080	420	20
0.4	/	2708	501	50
0.45	/	5087	651	153
0.5	8936	/	/	763

clear that the present method has distinct advantages on the computational time compared with the Voronoi-based method [11] and the traditional random aggregate method [19]. Especially when the volume fraction of aggregates is less than 40%, the present method can directly generate the meso-scale finite element model of concrete within 1 min.

In addition, the conventional concrete meso-modelling method has an obvious shortcoming. The volume fraction of aggregate elements of the meso-scale finite element model will be much smaller than that of the meso-scale geometric model. As mentioned in reference [4], the aggregate content of the meso-scale geometric model is 58.9%, while the actual contents of aggregate elements of the corresponding meso-scale finite element models are only 31.0% and 25.0%, respectively. However, in present method, since the meso-scale finite element model of concrete is directly established without generating the meso-scale geometric model, the final volume fraction of the aggregate elements in the meso-scale finite element model is exactly the predefined value of aggregate content.

4.2. Case analysis

According to the concrete meso-modelling process of this paper, the corresponding C++ program is implemented on a desktop computer with Intel Core i5@3.2 GHz and 4 GB memory. In the subsequent case analysis, all the meso-scale finite element models of concrete are built in a target space with a three-dimensional size of 100 mm × 100 mm × 100 mm. The influences of aggregate element content, mesh element size and aggregate particle size distribution on the concrete meso-modelling are analyzed.

In order to eliminate the influence of different amount of mesh elements, the actual computing time of concrete meso-modelling are normalized to be the normalized computing time. Taking 1 million mesh elements as the reference value, for the case with a total element number of 8 million and the actual computing time $t_m = 16$ s, the corresponding normalized computing time will be $t_m = 2$ s.

4.2.1. The effect of aggregate content

Consider the following situations, the element size of the meso-scale finite element model is 0.5 mm, the aggregate particle size distribution is 24 ~ 4 mm, and the aggregate element contents are 30%, 35%, 40%, 45% and 50%, respectively. Fig. 7 illustrates the meso-finite element model, mortar, aggregate and ITZ of concretes as well as the corresponding three-dimensional symmetrical slices, when the contents of aggregate element is 50%. With the increase of the aggregate element content, the ITZ element content increases and the mortar element content decreases, as shown in Fig. 8. It can be seen from Fig. 9 that as the aggregate element con-

tent increases, the time of generating the concrete meso-model increases almost exponentially.

4.2.2. The effect of element size

Consider the following situations, the aggregate element contents of the concrete meso-finite element model are 40% and 50%, the aggregate particle size distribution is 24 ~ 4 mm, and the element sizes are 0.5 mm, 0.8 mm and 1 mm, respectively. Fig. 10 illustrates the concrete meso-finite element model, mortar, aggregate and ITZ of the coarse element (1 mm, case 2-1), as well as the corresponding three-dimensional symmetrical slices, respectively. Under the case of same aggregate element content and aggregate particle size distribution, the smaller the element size, the lower the ITZ element content and the higher the mortar element content, as shown in Fig. 11. As the element size decreases, the total number of mesh elements increases, which makes the actual time of concrete meso-modelling longer. However, the scaling time of concrete meso-modelling becomes shorter, which indicates that the finer element mesh is more conducive to the successful placement of aggregates in the background grid, as shown in Fig. 12.

4.2.3. The effect of aggregate particle size distribution

Consider the following situations, the element size of the concrete meso-finite element model is 1 mm, the aggregate element content is 40%, and the aggregate particle size distributions are 24 ~ 4 mm, 20 ~ 4 mm, 16 ~ 4 mm and 12 ~ 4 mm, respectively. Fig. 13 illustrates the concrete meso-finite element model, mortar, aggregate and ITZ, as well as the corresponding three-dimensional symmetrical slices when the aggregate particle size is relatively small (12~4 mm). Fig. 14 shows that under the same element size and aggregate element content, the wider the aggregate particle size range, the lower the ITZ element content and the higher the mortar element content. As can be seen from Fig. 15, the wider the aggregate particle size range, the shorter time required to generate the concrete meso-model, showing an exponential downward trend.

5. Validation of numerical simulations

In this section, the concrete meso-model generated in this paper will be used to perform the mesoscopic numerical simulation of concrete uniaxial compression and projectile penetration through the general finite element code LS-DYNA to verify the effectiveness of the concrete meso-model.

5.1. Uniaxial static compression test

The 3D meso-finite model of concrete under uniaxial static compression is shown in Fig. 16. A standard cubic concrete meso-finite

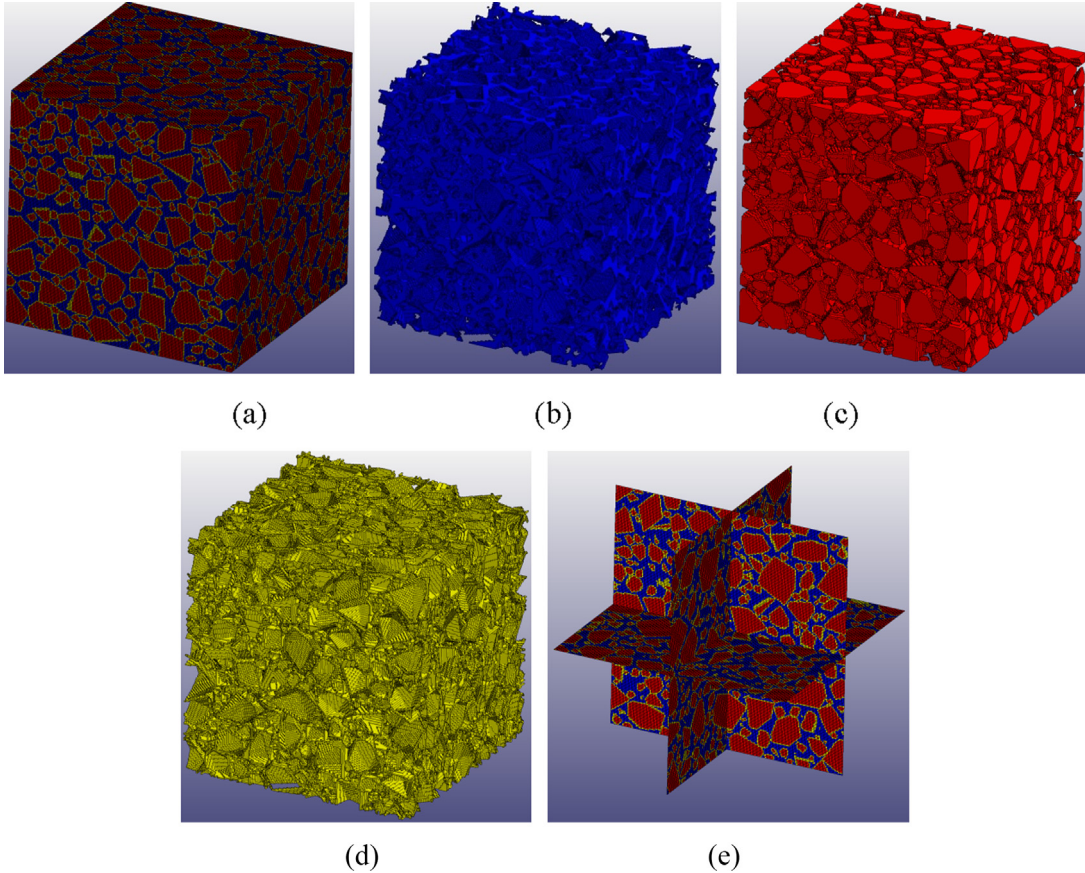


Fig. 7. The concrete meso-model with 50% aggregate element content (case 1–5): (a) meso-finite element model, (b) mortar, (c) aggregate, (d) ITZ, (e) three-dimensional symmetrical slices.

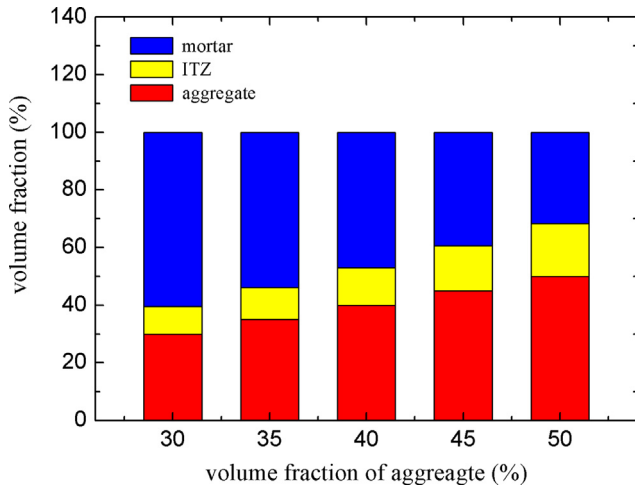


Fig. 8. The effect of aggregate content on the content of meso-components of concrete.

model with the size of 150 mm is established in the compression simulation. The mesh element size is 1.5 mm, and the aggregate element content is 40%. The maximum and minimum aggregate size are 20 mm and 6 mm, respectively. The upper and lower rigid plates have smooth contact with concrete specimen.

In present simulation, the K&C concrete damage model is employed for aggregate, mortar and ITZ. This material model introduces three failure surfaces, namely the initial yield surface, ultimate strength surface, and residual strength surface, and it is

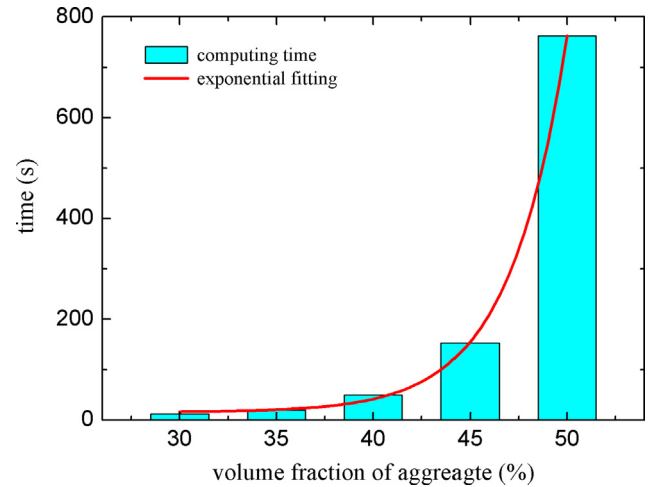


Fig. 9. The effect of aggregate content on the time of generating the concrete meso-model

capable of describing the effects of strengthening, tensile and compressive damage, volume deformation damage, and strain rate of concrete-like materials.

For normal concrete, aggregates are generally crushed stones of varying strength, but are much stronger than mortar. The strength of mortar is usually not much different from the unrestrained compressive strength of concrete. Especially, the material properties of ITZ layer are difficult to determine precisely. It is generally

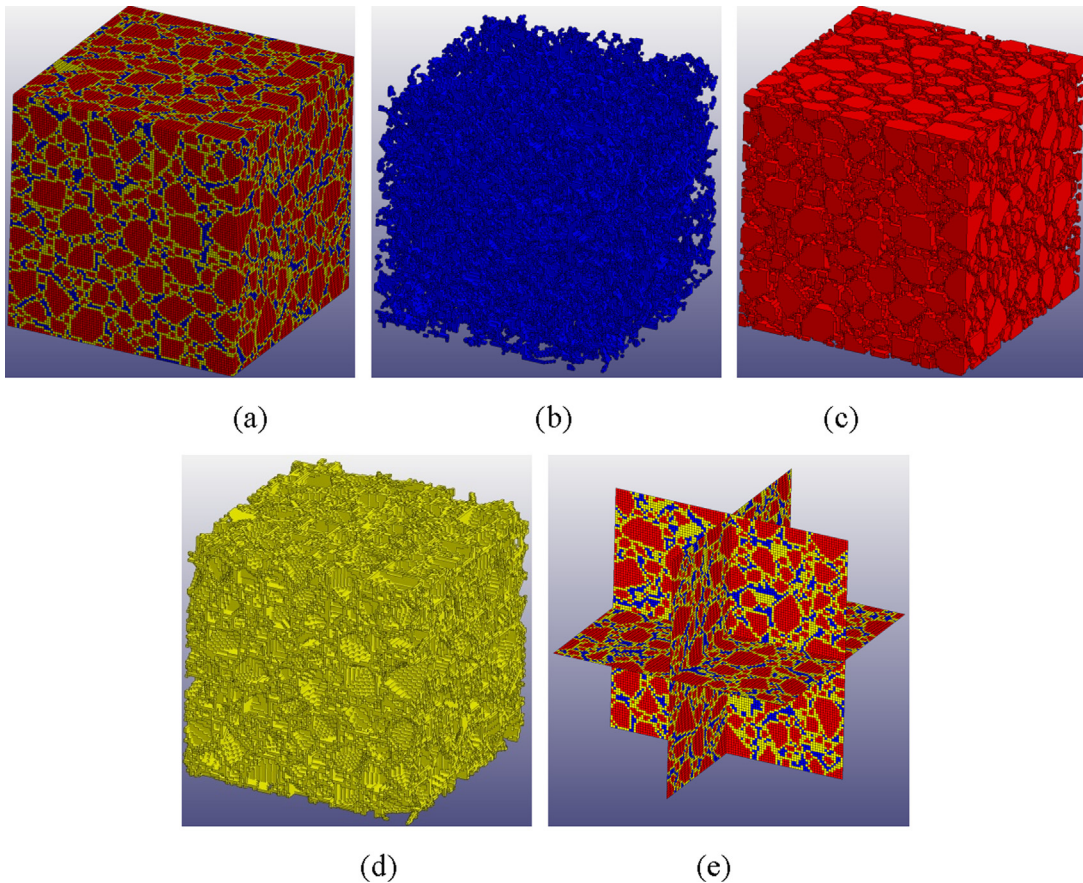


Fig. 10. The concrete meso-model of coarse element size (1 mm, case 2-1): (a) meso-finite element model, (b) mortar, (c) aggregate, (d) ITZ, (e) three-dimensional symmetrical slices

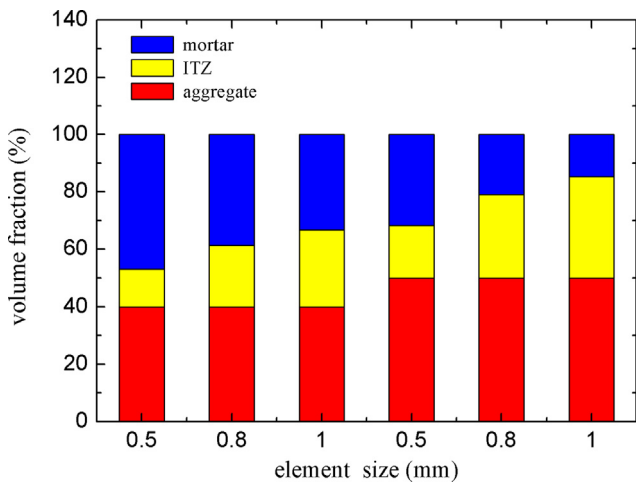


Fig. 11. The effect of element size on the content of meso-components of concrete

believed that ITZ is weaker than mortar and has about half the strength of mortar. Through repeated parametric trial numerical tests, the main material parameters for aggregate, mortar and ITZ are determined in present simulation, as shown in [Table 3](#), where ρ is material density, μ is Poisson's ratio, σ_c indicates the compressive strength, ε_{\max} is the maximum principal strain at failure, and f_c represents the unconstrained compressive strength of concrete.

Fig. 17 shows the contours of the maximum principal strain of the meso-scale concrete at different nominal strain. With the con-

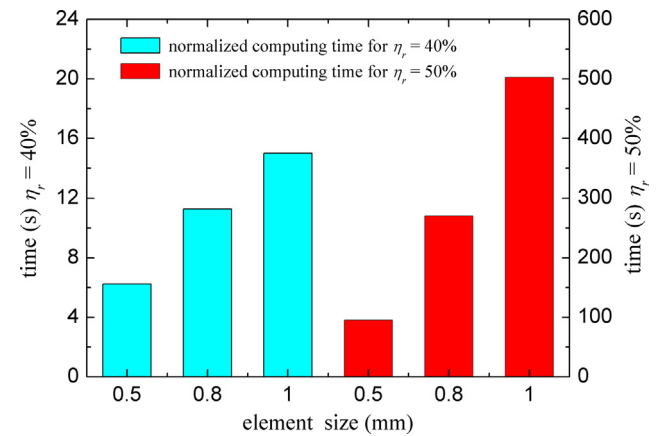


Fig. 12. The effect of element size on the scaling time of concrete meso-modeling

tinuous compression of concrete, the tensile strain damage caused by the compressive expansion effect will be accumulated, and it is mainly concentrated in the weakest region along the ITZ. Eventually, cracks develop along the ITZ, and are basically parallel to the loading direction. Compared with the *meso*-scale concrete in Fig. 16, it is clear that the distribution of ITZ has an important impact on the distribution and development of cracks. The simulated compressive stress-strain curve shows good agreements with the experimental results [20] when the compressive strength is 48 MPa, as shown in Fig. 18.

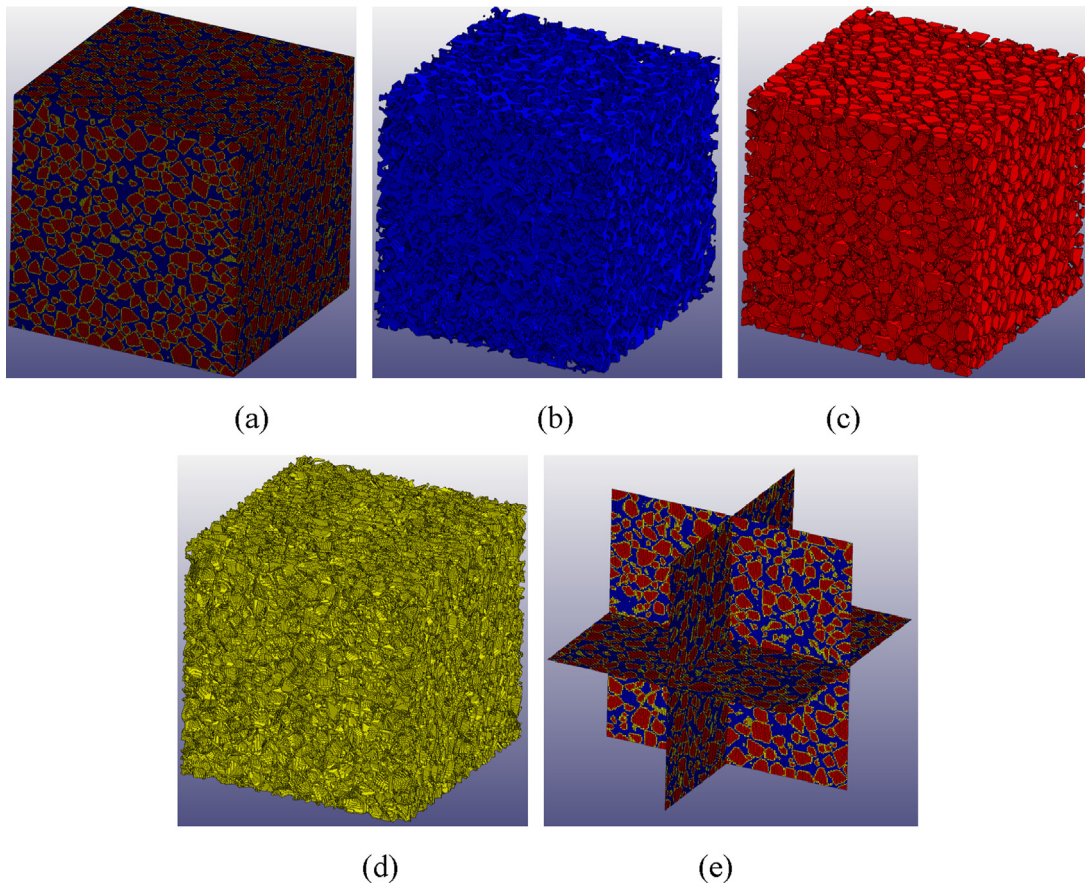


Fig. 13. The concrete meso-model with small aggregate particle size (12~4 mm, case 3~4): (a) meso-finite element model, (b) mortar, (c) aggregate, (d) ITZ, (e) three-dimensional symmetrical slices

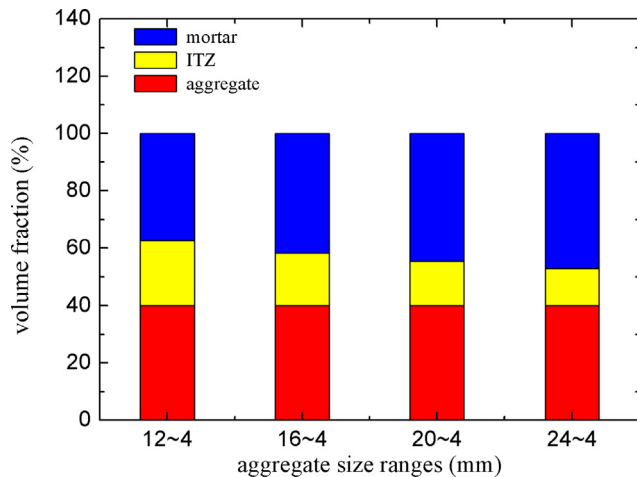


Fig. 14. The effect of aggregate size distribution on the content of meso-components of concrete

Under the same conditions, three random meso-scale models of concrete with an unconstrained compressive strength of 62.8 MPa were generated to analyze the effect of randomness of aggregate placement on the stress-strain curve of uniaxial compression. Fig. 19 shows the nominal stress-strain curves of three random meso-scale models of concrete. It demonstrates that the randomness of the concrete meso-scale model only slightly affects the post-peak section of the compressive stress-strain curve.

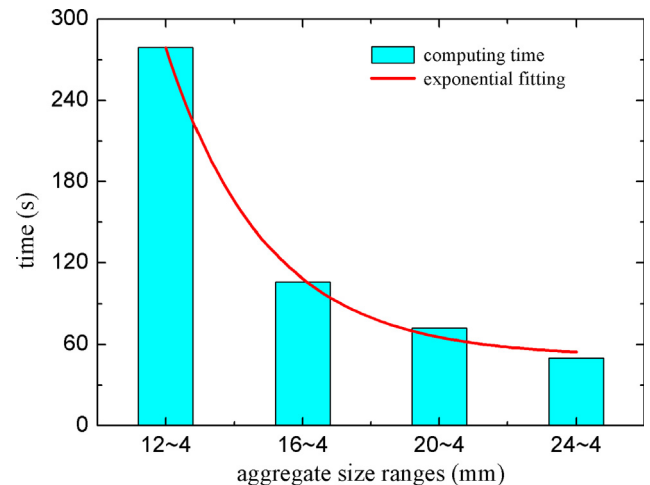


Fig. 15. The effect of aggregate size distribution on the time of concrete meso-modelling

5.2. Verification of projectile penetration into concrete target

In this section, we conducted numerical simulation of the tests by Forrestal et al. [21] to verify the reliability of the meso-scale finite model of concrete established based on present method. In these tests, the diameter of projectile body is 20.3 mm, the length-diameter ratio of projectile is 10, the CRH value of the ogival projectile nose is 3.0, and the initial penetrating velocities of the

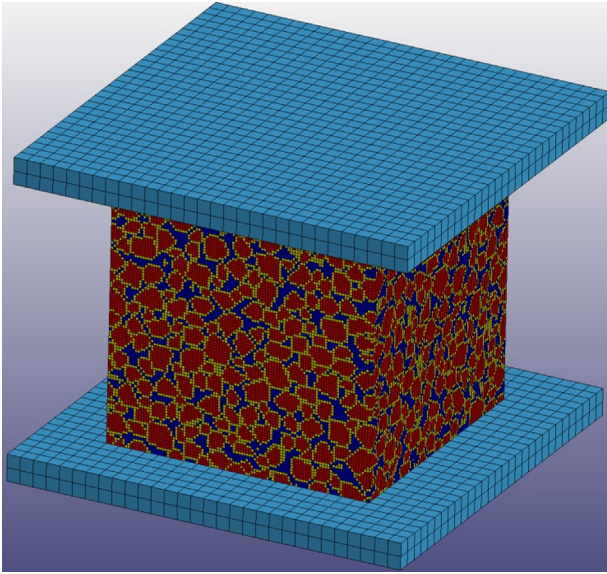


Fig. 16. The meso-scale finite element model of concrete under uniaxial compression

projectile are 415 m/s, 612 m/s, 821 m/s, 926 m/s and 987 m/s, respectively. The unconstrained compressive strength of the concrete target is 62.8 MPa. The material parameters of concrete meso-scale components are obtained by the uniaxial compression simulation in the previous section. With the increase of the initial penetration velocity, the penetration depth of the projectile increases, so the size of the meso-scale finite element model of the concrete

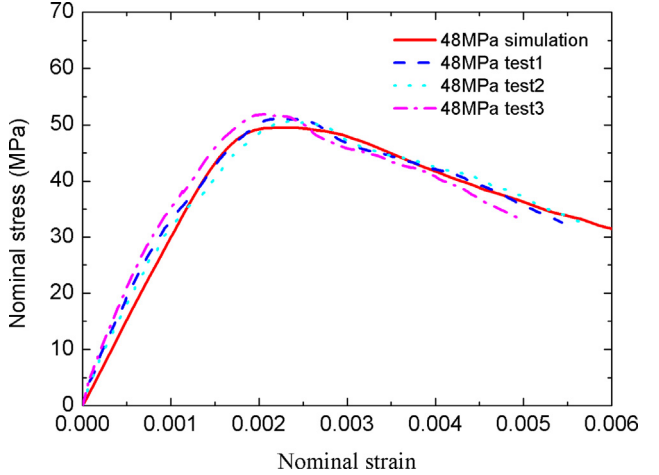


Fig. 18. Nominal stress-strain curve of concrete in comparison with typical experimental results [20]

target also needs to increase accordingly. **Fig. 20** shows the concrete meso-scale model when the initial penetrating velocity of projectile is 612 m/s.

As can be seen from **Fig. 21**, the failure mode of concrete is asymmetrical due to the heterogeneity of the meso-scale concrete target. The projectile deflects and inclines during penetration, and the trajectory deflects obviously. The curves of penetration depth versus time and corresponding acceleration versus time of the penetrator are shown in **Fig. 22**. Good agreement can be obtained from **Fig. 23**, especially when the initial penetration speed is less than 800 m/s, where the assumption of a rigid projectile still applies.

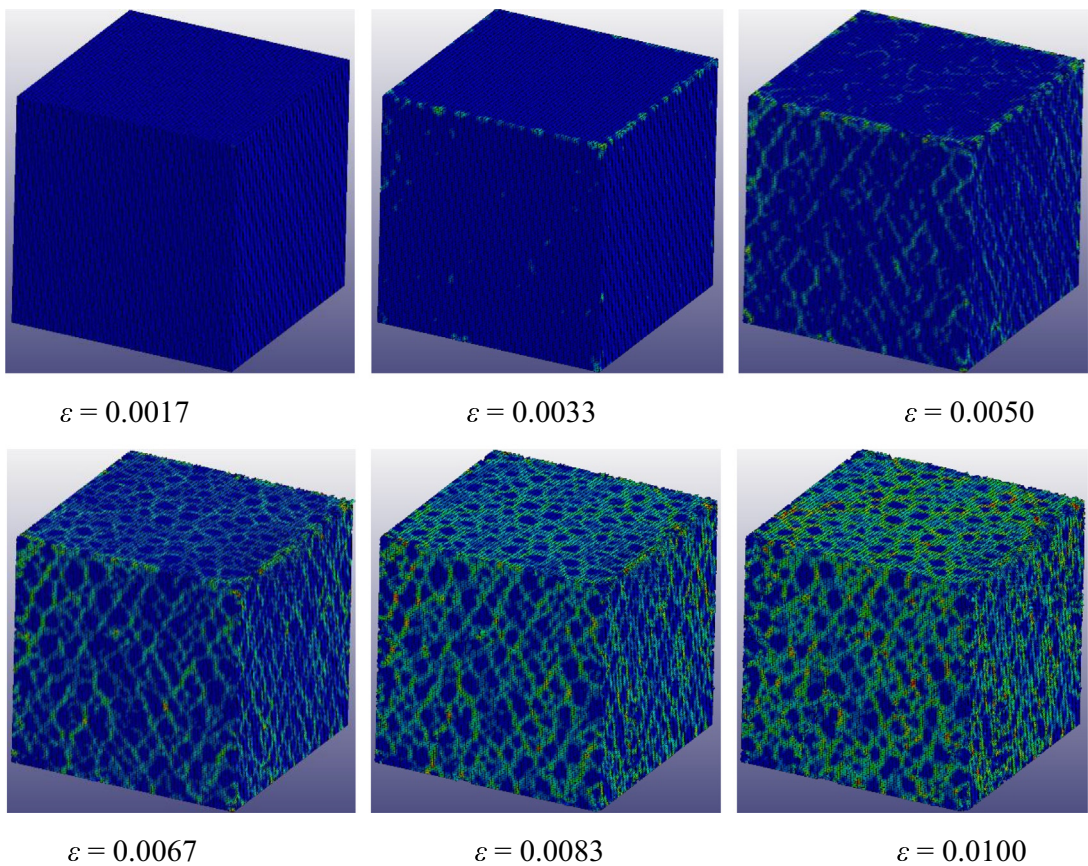


Fig. 17. Contours of the maximum principal strain at different nominal strains

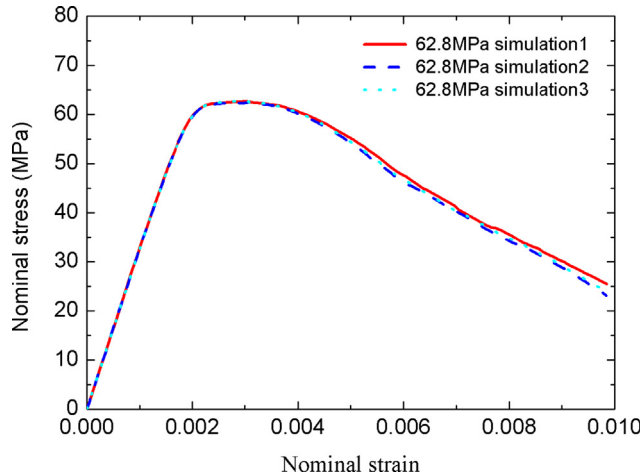


Fig. 19. Nominal stress-strain curves of three random meso-scale models of concrete under the same meso-modelling conditions

The results show that the *meso*-model of concrete established in this paper is reliable and effective.

6. Conclusions

In this paper, a novel and comprehensive method has been developed to directly generate *meso*-finite element model of concrete based on the local background grid method, which simplifies the traditional process of concrete *meso*-modeling and improves the efficiency distinctly.

The procedure presented in this paper is applicable to both 2D and 3D situations, and has no restrictions on the shape of aggregates, including circular, elliptical, polygonal, spherical, ellipsoidal and polyhedral, or even non-convex polygonal or polyhedral aggregate. Reinforcement steel can also be pre-introduced into concrete model as a special shape aggregate to build the *meso*-scale model of reinforced concrete.

In this paper, the aggregate content is the actual volume content in the concrete *meso*-model. In contrast to other *meso*-modeling methods, the present method is more efficient and can achieve higher aggregate content.

Table 3
Material parameters.

Component	ρ (kg/m ³)	μ	ε_{\max}	σ_c (when $f_c = 48$ MPa)(MPa)	σ_c (when $f_c = 62.8$ MPa)(MPa)
aggregate	2600	0.2	0.15	100	100
mortar	2200	0.2	0.15	45	59
ITZ	2000	0.23	0.15	27	35

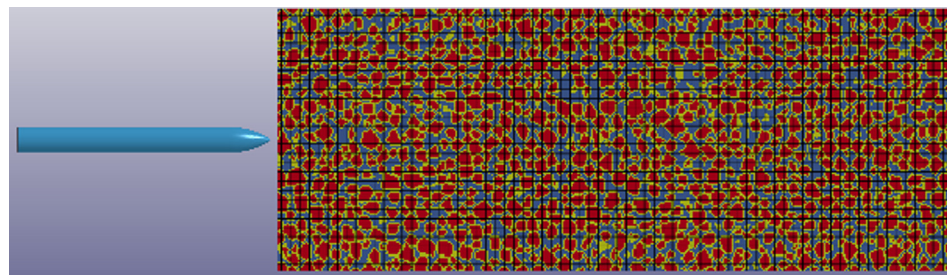


Fig. 20. Finite element model of projectile penetrating meso-scale concrete target at the initial penetrating speed of 612 m/s

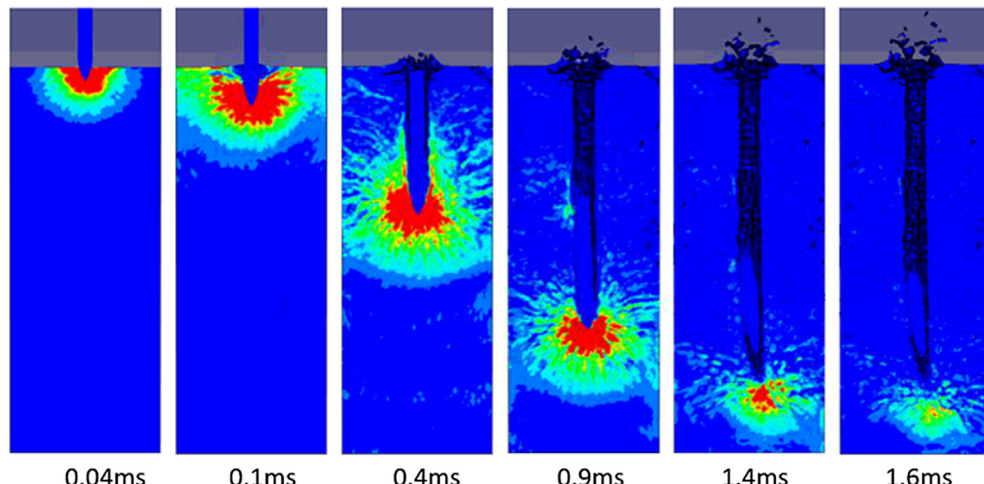


Fig. 21. Penetration process of projectile penetrating into the meso-scale concrete target at the initial penetrating speed of 612 m/s

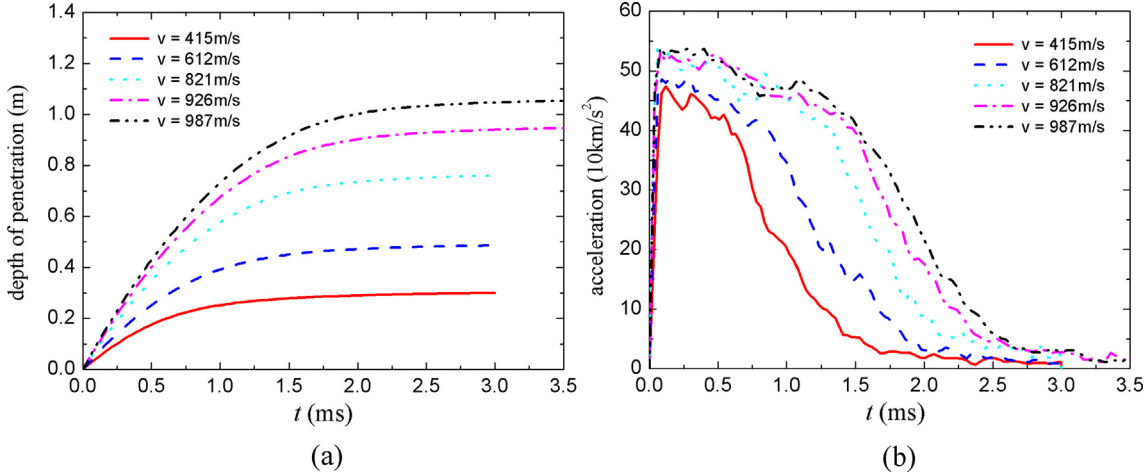


Fig. 22. Projectile penetrating meso-scale concrete target: (a) penetration depth versus time, (b) acceleration versus time

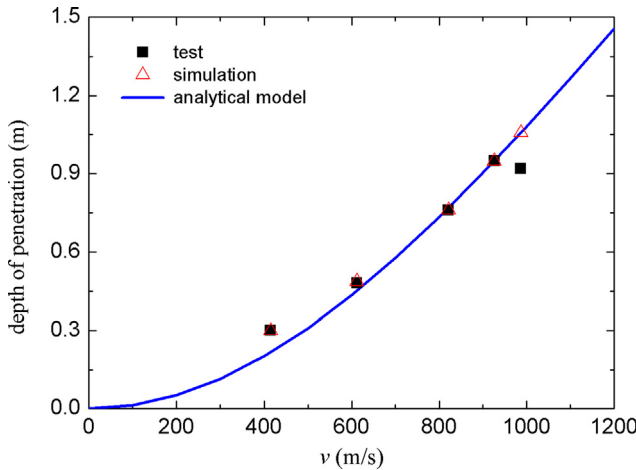


Fig. 23. Comparison of simulated penetration depths with experimental results [21] and the analytical model of rigid projectile

According to the results of case analysis, the aggregate content of the meso-model is up to 50%. For a finer background mesh and a wider aggregate particle size range, the aggregate content can be even higher.

The compression and penetration simulations are carried out based on the concrete meso-model established in this paper. The results can qualitatively explain the influence of the meso-structure on the macro-mechanical behavior of concrete.

Declaration of Competing Interest

The authors declare that they have no known competing financial interests or personal relationships that could have appeared to influence the work reported in this paper.

Acknowledgment

This work was supported by the National Natural Science Foundation of China (11627901, 11872118).

References

- [1] Y. Lu, Z. Tu, Mesoscale modelling of concrete for static and dynamic response analysis Part 2: Numerical investigations, *Struct. Eng. Mech.* 37 (2) (2011) 215–231.
- [2] Q. Fang, J.H. Zhang, Y. Huan, Y.D. Zhang, Research on modeling method of 3D meso-model of full-grade concretes, *Eng. Mech.* 30 (1) (2013) 14–21 (Chinese).
- [3] Y.C. Li, H.F. Ma, H.Q. Chen, X. Hu, Approach to generation of random convex polyhedral aggregate model and plotting for concrete meso-mechanics, *J. Hydraul. Eng.* 37 (5) (2006) 588–592 (Chinese).
- [4] H.F. Ma, W.X. Xu, Y.C. Li, Random aggregate model for mesoscopic structures and mechanical analysis of fully-graded concrete, *Comput. Struct.* 177 (2016) 103–113.
- [5] X. Wang, M. Zhang, A.P. Jivkov, Computational technology for analysis of 3D meso-structure effects on damage and failure of concrete, *Int. J. Solids Struct.* 80 (2016) 310–333.
- [6] A. Yin, X. Yang, C. Zhang, G. Zeng, Z. Yang, Three-dimensional heterogeneous fracture simulation of asphalt mixture under uniaxial tension with cohesive crack model, *Constr. Build. Mater.* 76 (2015) 103–117.
- [7] N. Benkemoun, M. Hautefeuille, J.B. Colliat, A. Ibrahimbegovic, Failure of heterogeneous materials: 3D meso-scale FE models with embedded discontinuities, *Int. J. Numer. Meth. Eng.* 82 (13) (2010).
- [8] A. Caballero, C.M. López, I. Carol, 3D meso-structural analysis of concrete specimens under uniaxial tension, *Comput. Methods Appl. Mech. Eng.* 195 (52) (2006) 7182–7195.
- [9] S.A. Galindo-Torres, D.M. Pedroso, D.J. Williams, L. Li, Breaking processes in three-dimensional bonded granular materials with general shapes, *Comput. Phys. Commun.* 183 (2) (2012) 266–277.
- [10] K. Nagai, Y. Sato, T. Ueda, Mesoscopic Simulation of Failure of Mortar and Concrete by 3D RBSM, *J. Adv. Concr. Technol.* 3 (3) (2005) 385–402.
- [11] J. Zhang, Z.Y. Wang, H.W. Yang, Z.H. Wang, X.F. Shu, 3D meso-scale modeling of reinforcement concrete with high volume fraction of randomly distributed aggregates, *Constr. Build. Mater.* 164 (2018) 350–361.
- [12] Y.J. Huang, Z.J. Yang, W.Y. Ren, G.H. Liu, C.Z. Zhang, 3D meso-scale fracture modelling and validation of concrete based on in-situ X-ray Computed Tomography images using damage plasticity model, *Int. J. Solids Struct.* 67–68 (2015) 340–352.
- [13] H.K. Man, J.G.M.V. Mier, Damage distribution and size effect in numerical concrete from lattice analyses, *Cem. Concr. Compos.* 33 (9) (2011) 867–880.
- [14] R. Zhou, Y. Lu, 3D mesoscale finite element modelling of concrete, *Comput. Struct.* 192 (2017) 96–113.
- [15] Z.M. Wang, Z.Z. Qiu, Random aggregate structure of mesoscopic concrete and finite element mesh, *Chinese Journal of Computational Mechanics* 22 (6) (2005) 728–732 (Chinese).
- [16] P. Wriggers, S.O. Mofat, Mesoscale models for concrete: Homogenisation and damage behaviour, *Finite Elem. Anal. Des.* 42 (7) (2006) 623–636.
- [17] Fuller W B, Thompson S E. The laws of proportioning concrete. The American Society of Civil Engineers. Transactions of American Society of Civil Engineers. Vol. LIX, 1926: 67–172.
- [18] X.W. Tang, C.H. Zhang, Layering disposition and FE coordinate generation for random aggregate arrangements, *Journal of Tsinghua University (Science and Technology)* 12 (2008) 2048–2052 (Chinese).
- [19] T.H. Lv, X.W. Chen, G. Chen, The 3D meso-scale model and numerical tests of split Hopkinson pressure bar of concrete specimen, *Constr. Build. Mater.* 160 (2018) 744–764.
- [20] A. Rajput, M.A. Iqbal, Impact behavior of plain, reinforced and prestressed concrete targets, *Mater. Des.* 114 (2017) 459–474.
- [21] M.J. Forrestal, D.J. Frew, S.J. Hanchak, N.S. Brar, Penetration of grout and concrete targets with ogive-nose steel projectiles, *Int. J. Impact Eng.* 5 (1996) 465–476.